Thermochimica Acta 510 (2010) 53–60

Contents lists available at ScienceDirect

Thermochimica Acta

journal homepage: www.elsevier.com/locate/tca

Calorimetric measurement of the heat generated by a Double-Layer Capacitor cell under cycling

C. Pascot, Y. Dandeville, Y. Scudeller*, Ph. Guillemet, T. Brousse

Université de Nantes, Ecole Polytechnique, LGMPA, La Chantrerie, rue Christian Pauc, BP 50609, 44306 Nantes Cedex 3, France

ARTICLE INFO

Article history:
Received 7 December 2009
Received in revised form 24 April 2010
Accepted 22 June 2010
Available online 17 July 2010

Keywords:
Double-Layer Capacitor
Supercapacitor
Power dissipation
Calorimetry
Thermal analysis

ABSTRACT

A calorimetric technique was developed for measuring heat generated within a Double-Layer Capacitor cell under cycling by analyzing its transient temperature change. Measurements were performed for a short time period of the current cycle to get small temperature changes and thus not substantially affect the properties of the cell during charge and discharge. The calorimetric technique is described and its performance demonstrated on a symmetrical activated carbon cell with 1 M $N(C_2H_5)4BF_4$ in propylene carbonate as electrolyte over a wide current range. Capacitance of the cell at room temperature was around to 0.25 F cm^{-2}. Power density was found between 2×10^{-3} to 70×10^{-3} W cm^{-2} according to the current density that varied between 0.01 and 0.15 A cm^{-2} for a cell load pressure equal to 25 kg cm^{-2}. Equivalent resistance, measured on the calorimeter, was found to vary between 4 and 8 Ω cm^2, according to the charge rate. Calorimetric measurements were found in good agreement with the energy balance of the cell deduced from the potential profiles and currents.

1. Introduction

Double-Layer Capacitors are energy storage devices intermediate between rechargeable batteries and electrolytic capacitors with respect to energy and power performance [1]. They are attractive for many applications such as the power back-up for memory functions, the peak power assistance to reduce the duty-cycle on a battery, as well as temporary energy storage in Electric Vehicles [1,2,3,4]. A symmetric Double-Layer Capacitor cell consists of two identical porous electrodes coated on metal current collectors, and a polymer separator between them wetted with a liquid electrolyte, as shown in Fig. 1. For a carbon Double-Layer Capacitor, the charge storage is mainly achieved by electrostatic interactions through the electrochemical-double-layer between the high surface-area electrode and the electrolyte. Upon charge and discharge cycling, a fraction of the energy exchanged within the cell is dissipated into heat, in the volume of the active materials and the electrolyte (see Fig. 1). Heat generation is mainly caused by Joule losses due to the resistive paths existing through the porous solid matrix and the pores of the cell filled with the liquid electrolyte (carbon electrodes, separator). Reversible and irreversible heat due to electrochemical reactions, entropy change [5], and dielectric losses [6] can be generally neglected.

Nowadays, there is a demand for producing cells offering suitable performance at high charge rates over a wide temperature range. Power dissipation remains one of the key factors affecting safety and reliability. Dissipated power is required for predicting temperature and estimating energy efficiency [12]. Indeed, calorimetric techniques offer an interesting direct route for determining the heat generated by various energy storage devices such as rechargeable batteries and dielectric capacitors (see for example [7–10]). Calorimetric techniques can also contribute to a better understanding of the electrochemical processes.

This paper presents a calorimetric technique developed for measuring heat generated within electrochemical capacitors cells under cycling. The calorimetric technique and the experimental apparatus are described. The heat generation rate of a carbon Double-Layer Capacitor cell was measured as a function of charge rates. The results are reported and discussed.

2. Experimental

A heat conduction calorimetric technique was developed for determining heat generated within a Double-Layer Capacitor cell under cycling. The technique is based on transient temperature analysis of the cell after applying a charge-discharge current cycle. A schematic of the experimental apparatus is shown in Fig. 2. The cell under test /1/ was pressed between two heat-flux sensors /2/ attached to a reference cold plate /3/ symmetrically positioned (see Fig. 2). The reference cold plate /3/ was maintained at constant temperature by a fluid circulator /A/ operating in

* Corresponding author.
E-mail address: yves.scudeller@univ-nantes.fr (Y. Scudeller).

0040-6031/$ – see front matter © 2010 Elsevier B.V. All rights reserved.
doi:10.1016/j.tca.2010.06.022

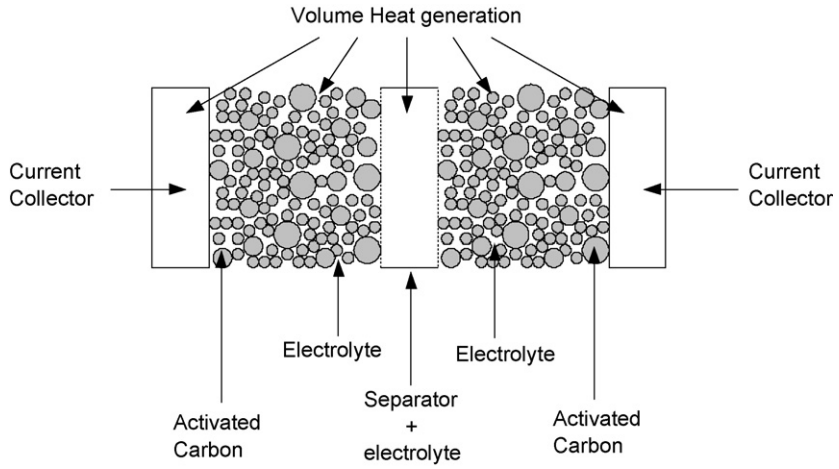

Fig. 1. Double-Layer Capacitor cell upon charge–discharge cycling. A volume heat is generated in each component of the cell.

the range −20 to +80 °C. The cell under test was connected to a Galvanostat–Potentiostat /B/. Temperature change of the sensing surface was measured for a short time period after starting the current cycles (galvanostatic cycling). Temperature was recorded with a suitable data acquisition system /C/. Before testing, the cell could be axially compressed with a mechanical system to a loading pressure between 1 and 200 kg cm^{-2} controlled by a force sensor. A schematic of a heat-flux sensor /2/ is represented in Fig. 3. Each sensor /2/ was formed with a plate in polymethylmethacrylate (PMMA) incorporating 8 K type thermocouples /4/ connected in series to measure the temperature difference between the sensing surface where the cell /1/ is placed and its reference cold plate /3/. The thickness and diameter of each plate were 20 and 80 mm, respectively. Hot junctions of thermocouples were positioned to the sensing surface over a circle line of 5 mm diameter. Electrical insulation was ensured by a 50 μm thick polymer film (see Fig. 3b). Cold junctions of the thermocouples were attached to the side of the polymer plate in contact with the reference cold plate /3/ (see Fig. 3a). Otherwise, an annular electrolyte holder was created to the bottom side of the sensing surface to prevent the depletion of ions from the electrolyte solution during tests. Moreover, the calorimeter was fully assembled to avoid contamination of the cell and evaporation of the electrolyte toward the surrounding medium. The calorimeter was suitable for various types of electrochemical cells having a surface-area comprised between 4 and 20 cm^2.

However, each heat-flux sensor was carefully calibrated by maintaining a constant temperature difference of 5 °C between the hot and cold junctions of thermocouples. Thermocouple sensitivity was 315 μV K^{-1} over the temperature range between −20 and +80 °C. Temperature change as small as 2×10^{-3} °C can be thus detected. Additionally, precision on temperature measured at the sensing surface could be improved by connecting in series the two sensors symmetrically positioned. The series arrangement allows the signal output to be amplified by a factor of two

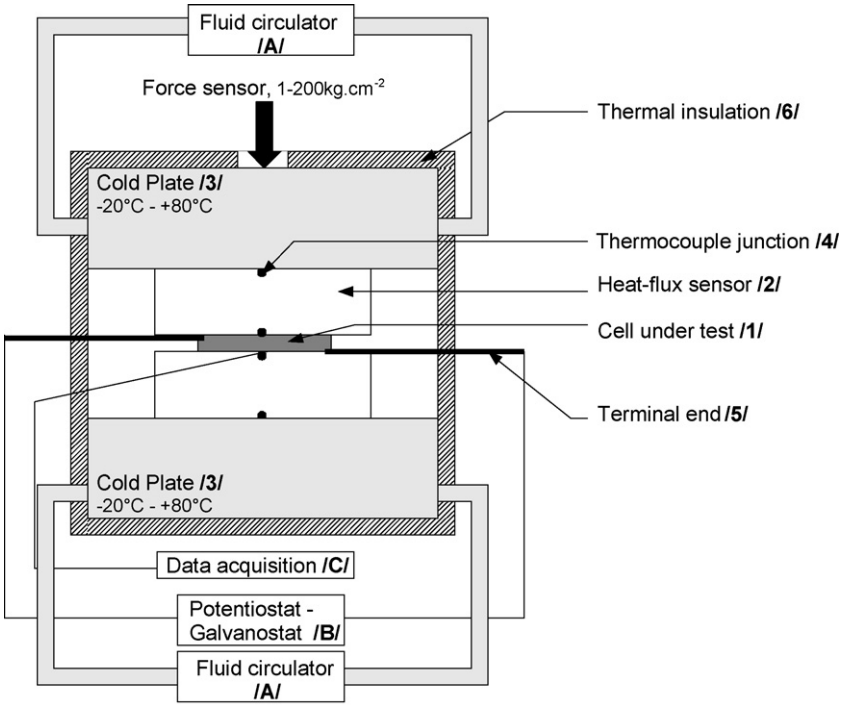

Fig. 2. Schematic of the calorimeter, as designed. /1/ Cell under test; /2/ heat-flux sensor; /3/ reference cold plate; /4/ thermocouple junctions; /5/ terminal ends for current collectors; /6/ thermal insulation; /A/ fluid circulator; /B/ Potentiostat–Galvanostat; /C/ data acquisition system.

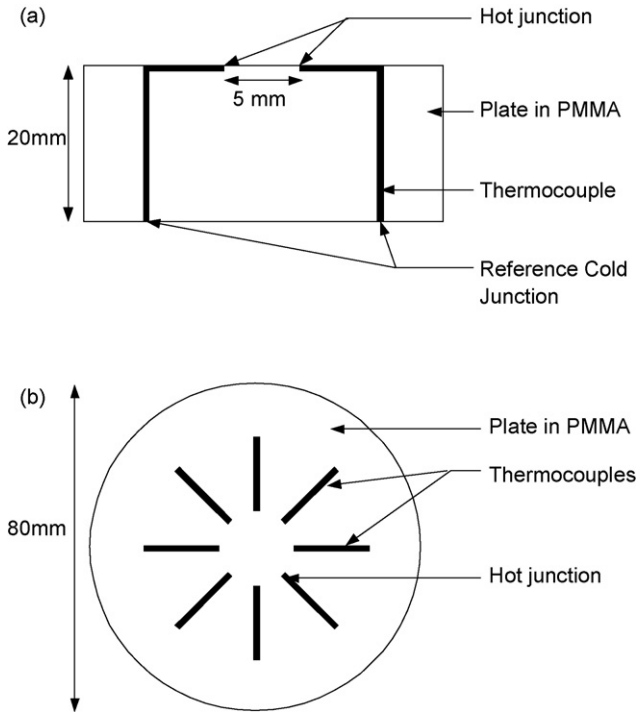

Fig. 3. Heat-flux sensor /2/, as fabricated. (a) Cross-section view; (b) top view.

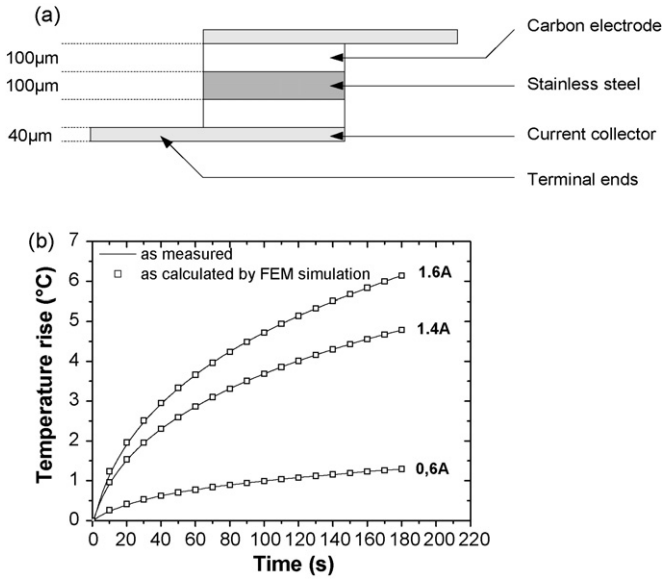

Fig. 4. Measurement on resistive cell. (a) Resistive cell construction; (b) calculated and measured temperature signals as a function of time for different applied currents (0.60, 1.40 and 1.60 A).

($630\,\mu V\,K^{-1}$). Moreover, thermal conductivity and volume heat capacity of the PMMA plate were measured to $0.20\,W\,m^{-1}\,K^{-1}$ and $1.818 \times 10^6\,J\,K^{-1}\,m^{-3}$, respectively (see Section 3).

Measurements can be achieved with small temperature change and thus ensure no significant thermal variation of the cell properties during charge. Temperature measurement was performed for a short time period after applying the current cycle in order to obtain a small temperature change. In practice, temperature increase was recorded for less than 300 s and the cell temperature did not generally exceed the initial temperature by more than couple of degrees Celsius, this being prescribed by the reference cold plates of the calorimeter. Heat generated was then estimated by fitting the cell temperature with a three-dimensional heat diffusion model. Dynamic temperature response of the cell was calculated by the Finite Elements Method (Comsol®-Multiphysics Software). The estimation procedure of the heat generation rate is discussed in Section 3.

The experimental apparatus is shown in Fig. 2. The calorimeter was numerically investigated to define suitable dimensions for the heat-flux sensors and the current collectors, in order to choose optimal thickness and width. Numerical simulations were carried out by considering the three-dimensional structure of the calorimeter and each component of the cell (current collectors, carbon electrodes, separator). A volume heat generation rate was considered.

First, it was found that the cell was isothermal in the cross-plane with a negligible thermal capacitance. The temperature difference in the cross-plane did not exceed 0.01 °C/W at any time of the temperature response for power density as high as $1\,W\,cm^{-2}$. On the other hand, as the current cycles were applied, the cell temperature varied in the plane direction due to the reduced surface of the cell, smaller than the sensors, which induced three-dimensional heat diffusion through the PMMA plates by causing such a temperature variation. Nevertheless, this variation was sufficiently small with regard to the cell temperature above the cold plate hat it did not substantially affect the precision of the calorimetric measurement. Thus, for instance, the temperature variation in the plane for a cell with 30 mm diameter was around 2 °C/W after 200 s, as the cell temperature above the cold plate was up to 20 °C/W. If the heat generation is $Q = 0.1$ W, then the variation in plane should not exceed 0.2 °C as the cell temperature is 2 °C above the cold plate. Moreover, one can mention that the terminal ends of the current collectors can also cause additional thermal paths in the plane because of the high thermal conductivity of aluminium compared with PMMA ($200\,W\,m^{-1}\,K^{-1}$ for aluminium versus $0.2\,W\,m^{-1}\,K^{-1}$ for PMMA). The dimensions of the current collectors were chosen to drastically limit the influence of the terminal ends on the cell temperature. For a better precision on the estimation of Q all three-dimensional effects described above have been considered for fitting temperature through a full numerical description of the calorimeter. A valuable temperature calculation was thus performed.

The calorimeter technology presented in this paper offers many advantages with regards to others such as differential scanning calorimetry and adiabatic calorimetry. At first, measurement used a suitable mechanical load at a constant pressure for controlling the electrical contacts and the density of the wet separator through the cell. Then, the calorimeter was totally tight to avoid the evaporation of the electrolyte. Next, the calorimeter was controlled in temperature and the cell temperature change should be sufficiently small to limit property variation. Such apparatus offers a route for the diagnostics of electrochemical cells of energy storage devices such as capacitors and batteries. The technique can achieve a better understanding of the electrochemical processes and conversion efficiency of such devices, as well as study degradation and aging mechanisms taking place at electrodes.

3. Results and discussion

3.1. Measurement on a resistive cell

The calorimetric technique was validated by applying different power steps within a cell acting as a constant resistor placed between the two heat-flux sensors, as described in Section 2. The resistive cell consists of a stainless steel sheet pressed between two carbon electrodes and two aluminium current collectors, as shown in Fig. 4a. Dimensions of the stainless steel sheet and each carbon electrode were 100 µm in thickness and 30 mm in diameter. The current collectors were chosen with a similar shape as

Table 1
Comparison between the temperature changes of the resistive cell versus time calculated with the Finite Elements Method and measured with the calorimeter (a) 0.6 A, 0.12 W; (b) 1.40 A, 0.48 W; (c) 1.60 A, 0.62 W.

Time (s)	Temperature variation (°C), as calculated	Temperature variation (°C), as measured	Relative error (%)
(a)			
20	0.416	0.39	−6.3
40	0.626	0.62	−0.96
60	0.776	0.77	−0.75
80	0.895	0.90	0.52
100	0.995	0.99	−0.59
120	1.083	1.08	−0.35
140	1.162	1.15	−1
160	1.232	1.23	−0.14
180	1.295	1.29	−0.4
(b)			
20	1.535	1.51	−1.65
40	2.305	2.29	−0.66
60	2.864	2.86	−0.14
80	3.313	3.31	−0.1
100	3.688	3.68	−0.23
120	4.013	4.01	−0.08
140	4.299	4.30	0.01
160	4.556	4.56	0.08
180	4.789	4.78	−0.20
(c)			
20	1.964	1.90	−3.3
40	2.956	2.93	−0.86
60	3.665	3.66	−0.14
80	4.240	4.24	−0.004
100	4.726	4.72	−0.13
120	5.144	5.14	−0.08
140	5.511	5.50	−0.2
160	5.841	5.83	−0.18
180	6.141	6.14	−0.01

the capacitor cell (see the following section). A step of constant current was applied through the cell with different rates. As the current cycle was applied in the cell, the heat generation rate, Q, was determined by fitting the temperature signal, measured into the calorimeter, with a model describing the heat diffusion process. A temperature signal was calculated by solving the heat diffusion equation with the Finite Elements Method within each component of the calorimeter by considering the cell exposed to a constant and uniform heat generation. In this way, Q was an input data of the model. Consequently, a temperature signal was derived for each value of Q addressed to the numerical model. Then, the value assigned for Q is obtained from a minimum in the least squares calculation. The calculated temperature signal is compared to the measured signal for a time period chosen around 300 s. Generally, the difference between the calculated and measured temperatures did not exceed 1%. This demonstrated that the temperature calculation was consistent with the calorimetric experiments. The calculation of the signal temperature used the thermal properties of PMMA as input data, the thermal properties of the cell being poorly sensitive to the signal. Thermal conductivity and diffusivity of PMMA have been measured with the Guarded Hot Plate Method and the Flash technique, respectively. Thermal conductivity It was calculated as $0.20 \pm 0.005\,W\,m^{-1}\,K^{-1}$ as and thermal diffusivity as $(1.1 \pm 0.01) \times 10^{-7}\,m^2\,s^{-1}$. A volume heat capacity of $(1.82 \pm 0.05) \times 10^6\,J\,K^{-1}\,m^{-3}$ was then derived. The thermal properties measured for PMMA were found in very good agreement with other reported values [13]. By considering the uncertainty of the PMMA properties, the precision on the calculated temperature was evaluated to be better than ±4%. Thus, the precision of the estimated value of Q, according the procedure described above, was estimated better than ±5%.

Table 2
Comparison between the power electrically measured on the resistive cell and the power measured with the calorimeter by temperature fitting.

	Applied current (A)		
	0.6	1.4	1.6
Power electrically measured (W)	0.12	0.48	0.62
Power measured with the calorimeter after fitting (W)	0.125	0.46	0.59
Relative difference (%)	4.2	4.4	4.8

Fig. 4 and Table 1 compare the calculated and measured temperature change between 0 and 180 s for three applied powers: 0.12, 0.48 and 0.62 W. Fig. 4 and Table 1 demonstrate a good agreement between the calculated and measured temperature signals. In Table 2, the calorimetric measurement of Q obtained with the procedure already described is compared with its value electrically measured from the relation $I \times V$, I and V denoting the current and the voltage between the collectors, respectively. As shown in Table 2, calorimetric measurement was found in good agreement with the electrical measurement. Differences did not exceed 5%.

Finally, numerical investigations and calibration tests have demonstrated that the accuracy of the calorimetric measurement of Q is better than 5%. Otherwise, detectable minimum power was assessed around 10×10^{-6} W (10 μW).

3.2. Measurement of Double-Layer Capacitor cell

A Double-Layer Capacitor cell was prepared under controlled atmosphere with two activated carbon electrodes. The specific surface area of the carbon particles was $650\,m^2\,g^{-1}$. Porous volume fraction was 64%. The electrodes were impregnated with 1 M $N(C_2H_5)_4BF_4$ salt dissolved in propylene carbonate. The cell is represented in Fig. 5. Electrode diameter and thickness was 30 mm and 100 μm, respectively. Thickness of the separator and current collectors were 35 and 40 μm, respectively. Average cell capacitance was around 1.7 Farad at room temperature. The cell was pressed between the two heat-flux sensors and then axially compressed to a constant loading pressure of $25\,kg\,m^{-2}$. Calorimetric measurements were performed under galvanostatic cycling with different current comprised between 0.1 and 1 A. As the cell surface area was about $7\,cm^2$, the current density applied was between 0.01 and $0.15\,A\,cm^{-2}$. High charge rates have been also applied to the cell to exacerbate its energy dissipation under cycling. Potential limitation was chosen to 2.0 V both for charge and discharge. Fig. 6a illustrates a current cycle applied to the cell at 0.4 A at 20 °C. Fig. 6b presents the cell voltage versus time, as measured for nine cycles after starting. Charge time was approximately equal to 3.5 s and cycle frequency was 0.15 Hz. Voltage profiles were found unchanged after approximately five charges. Table 3 gives the period and the frequency measured under the stabilized regime for each current applied. Fig. 7 illustrates the calorimetric measurement for the particular case presented in Fig. 6 (0.4 A current, 2 V potential window, 20 °C temperature). Fig. 7a gives the cell temperature versus time measured at 20 °C after applying the current cycle

Table 3
Period and frequency of the cell potential profile measured versus the charge–discharge current with 2.0 V as the potential window.

Current density ($mA\,cm^{-2}$)	14.3	28.6	42.9	57.1	71.4	85.7	100	114.3	128.6
Period (s)	54.8	21.6	15.8	6.8	4.0	2.3	1.5	1	0.6
Frequency (Hz)	0.02	0.05	0.06	0.15	0.25	0.44	0.7	1	1.7

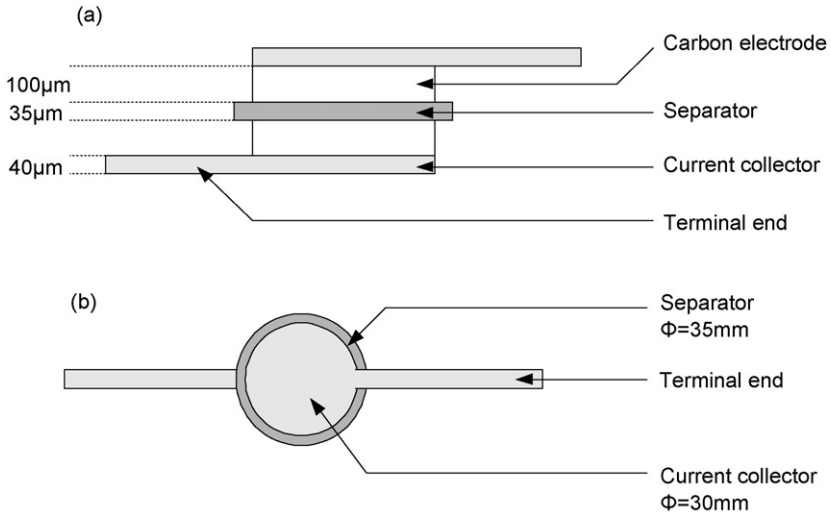

Fig. 5. Supercapacitor cell under test. (a) Cross-section view; (b) top view.

reported in Fig. 6a. For this particular case, the average power was estimated to 0.16 W by fitting the temperature signal over 200 s time for about 30 current cycles. After 200 s, it was found that the cell temperature increase does not exceed 2.5 °C. However, it can be noted that the cell temperature response exhibits oscillations with quite small amplitude (see Fig. 7a). Such temperature oscillations have already been observed for a carbon supercapacitor cell upon

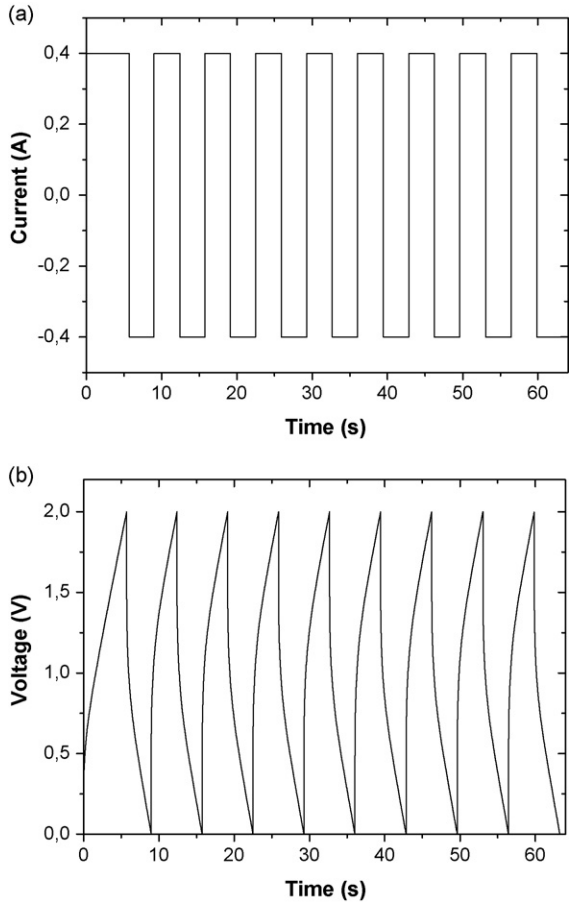

Fig. 6. Galvanostatic cycling, as applied for calorimetric measurements. (a) 0.4 A current cycle; (b) cell voltage versus time referring to the current cycle with 2.0 V as potential limitation.

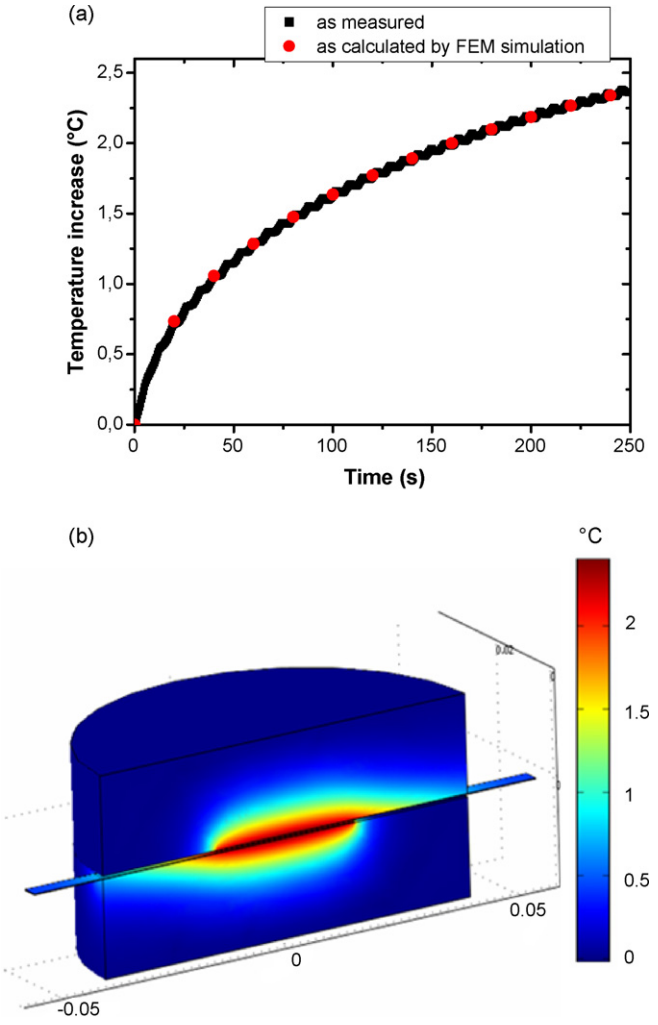

Fig. 7. Calorimetric measurement referring to the galvanostatic cycling shown in Fig. 6. (a) Calculated and measured temperature of the cell versus time; (b) temperature distribution of the calorimeter at 250 s time, as calculated by the Finite Elements Method.

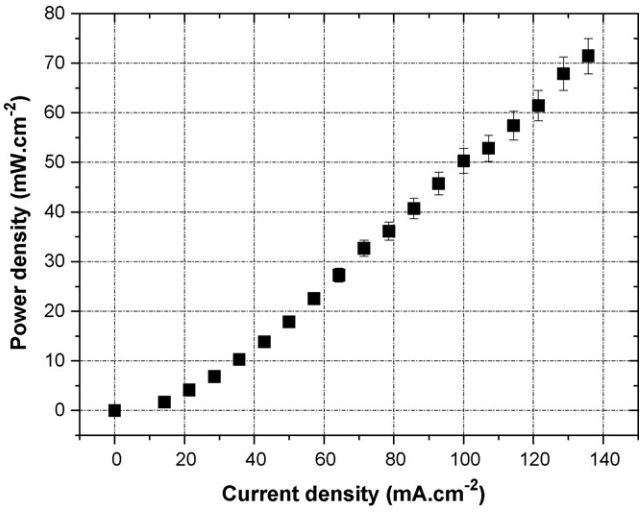

Fig. 8. Power density generated within the Double-Layer Capacitor cell measured by the calorimetric technique, as a function of the current density.

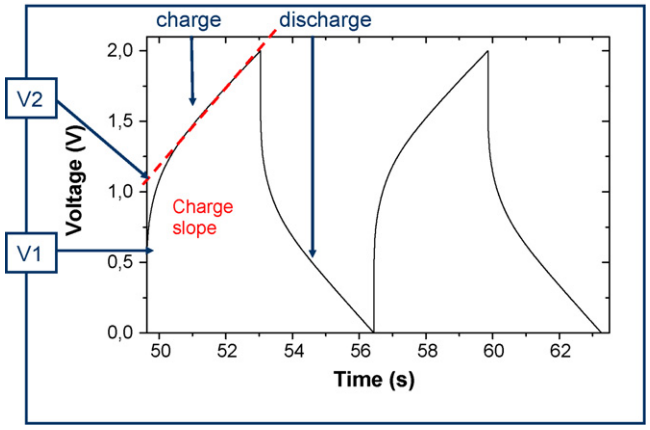

Fig. 9. Cell potential profile versus time for 0.4 A current and 2.0 V as potential window. V_1: potential offset referring to the separator; $V_2 - V_1$: potential offset at the electrodes.

charge–discharge cycling [5]. They were interpreted as a reversible effect due to the entropy change for the ions in solution taking place both on charge and discharge [5]. This thermal effect is quite small (approximately 5% of the change) and will not be considered in the present study. This phenomenon is under investigation. Fig. 7b shows the average temperature distribution within the calorimeter, calculated by the Finite Elements Method, at 200 s time after starting the current cycle. One observes that a small volume of the heat-flux sensors was exposed to the temperature increase (see Fig. 7b).

As already mentioned in Section 2, for all applied current, the heat generation rate was fitted in a time domain where temperature change remains sufficiently small to have no significant influence on the cell properties. Generally, for all charge rates, temperature rise did not exceed a couple of degree Celsius, as shown in Fig. 7 for 0.4 A as current. Temperature calculated by the Finite Elements Method was found in good agreement with measurements, as shown in Fig. 7. The thermal impedance referring to a cell diameter 30 mm was found around to 10 K W^{-1} at 200 s. In the steady state, the thermal impedance reaches 50 K W^{-1}.

Fig. 8 shows the heat generation rate Q measured at room temperature with the calorimetric technique as a function of the current density in the range 0.01–0.14 A cm^{-2}. According to the current, the heat generation rate Q was found between 0.01 and 0.5 W. Power density was comprised between 2×10^{-3} and 70×10^{-3} W cm^{-2} (see Fig. 8).

In addition, the heat generation rate Q measured by calorimetry was compared with the average power dissipated for a cycle, denoted as Q', electrically determined by considering the difference between the electrical energy supplied to the cell (in charge) and ones recovered from the cell (in discharge). Such energy represents the energy dissipated within the cell during a charge–discharge cycle. Generally, the dissipated energy could be transformed into different forms of energy by various physical and chemical processes. Q' is obtained by using relation (1) written as

$$Q' = \frac{E_{in} - E_{out}}{t_{charge} + t_{discharge}} \quad (1)$$

E_{in} denotes the electrical energy supplied to the cell during the charge time, t_{charge}, and E_{out} the energy removed from the cell during the discharge time $t_{discharge}$. E_{in} and E_{out} are given by relations (2) and (3), respectively as:

$$E_{in} = \int_{charge} IV\,dt \quad (2)$$

$$E_{out} = \int_{discharge} VI\,dt \quad (3)$$

E_{in} and E_{out} were determined after integrating the cell potential in time according to relations (2) and (3). Table 4 reports the values of Q', obtained from relation (1), and the heat generation rate Q, measured with the calorimeter for different charge rates comprised between 0.01 and 0.15 A cm^{-2}. Table 4 shows that Q' and Q are equal. It can be concluded that all the energy loss of the capacitor has been dissipated into heat. This result is consistent with the fact that the energy stored between a charge and a discharge should be much smaller than the thermal energy involved. High performance of the calorimeter was additionally confirmed.

Additional analysis was carried out by considering the potential offsets present in the potential signals versus time, as shown in Fig. 9, Reading the potential offsets offers a route for estimating the heat generated within each component of the capacitor. Fig. 9 gives a representative potential profile versus time for a charge–discharge cycle. Two potential offsets, denoted V_1 and V_2 in Fig. 9, can be observed for the charge. Because of the high electrical conductivity of the activated carbon with regard to the electrolyte, it is known that the electrical resistance of the electrodes before charging is much lower than the separator (see for example [11]). Thus, the potential offset V_1 (see Fig. 9) is due to the ionic resistance of the separator. Consequently, the formula $Q_1 = (I \times V_1)/2$ gives the power dissipated through the separator (I: current intensity). Fig. 10 presents Q_1 versus the current. As expected, Q_1 was found between 0.005 and 0.4 W ($(1–60) \times 10^{-3}$ W cm^{-2}) with values smaller than Q. Q_1 is a square function of the current, as shown in Fig. 10. The heat generated can be then deduced within the carbon electrodes Q_2 by calculating the difference $Q_2 = Q - Q_1$. Fig. 10 shows Q_2, plotted as a function of the current density. Moreover, the percentage of the heat generated within the separator and the electrodes with respect to Q, defined as Q_1/Q and Q_2/Q, are presented versus the current density in Fig. 11. It can be observed that, at low charge rate, Q_1 represents about 50% of the total heat and more than 90% at high rate. Thus, Q_2 remains in the same order of magnitude of Q_1 for current rates down to 50 mA cm^{-2} to reach about to 10% of the total heat for 150 mA cm^{-2}.

Otherwise, as already mentioned, the potential profile versus time exhibited an over-potential $V_2 - V_1$ (see Fig. 9) caused by the charge storage process that increases the effective resistance of the

Table 4
Comparison between the heat generation rates Q measured on the capacitor cell with the calorimeter and the power losses Q' determined with the electrical energy balance of the cell expressed in relations (1)–(3).

	Current density (mA cm^{-2})							
	28.6	42.9	57.1	71.4	85.7	100	114.3	128.6
Q' (W)	0.055	0.095	0.168	0.242	0.305	0.359	0.413	0.474
Q (W)	0.048	0.097	0.158	0.229	0.285	0.352	0.402	0.475

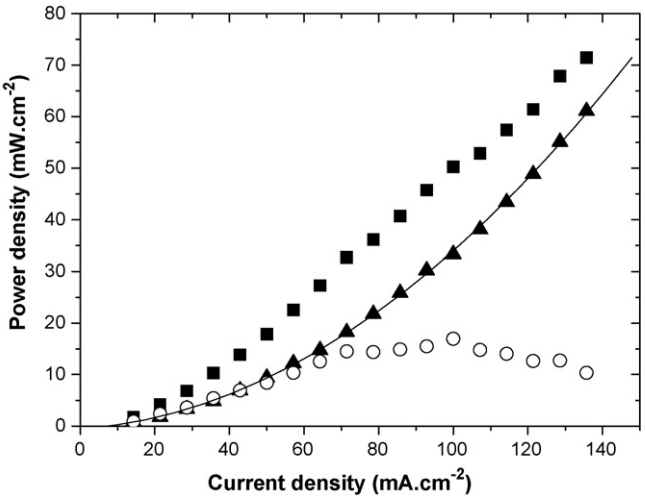

Fig. 10. Power density as a function of the current density. (■) Heat generated within the supercapacitor cell, measured with calorimetry, Q/S (▲) heat generated within the separator, measured with the potential offset V_1 (see Fig. 9), Q_1/S (○) heat generated within the carbon electrodes, defined as Q_2/S with $Q_2 = Q - Q_1$. As expected, power Q_1 was found as a square function of the current: $Q_1 = 0.47 \cdot I^2 + 6 \times 10^{-3}$ (continuous line).

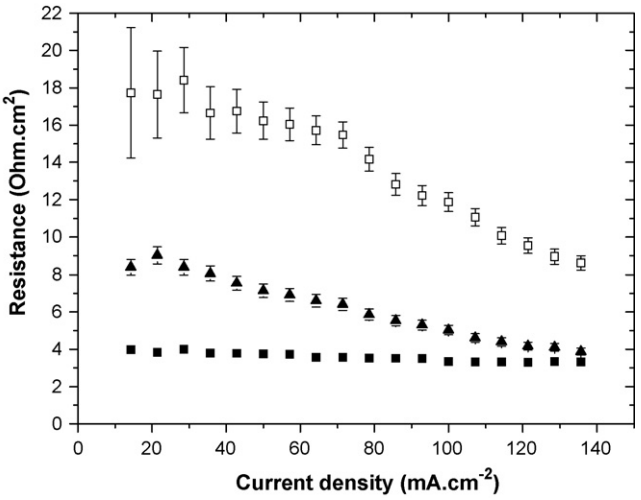

Fig. 12. Equivalent resistance per centimeter squared of the capacitor cell versus the current density, (▲), determined with calorimetry by using relation (4), denoted as R (■) referring to the separator, determined by relation (5), denoted as R_1 (□) referring to the charge offset, determined by relation (6), denoted as R_3.

electrode [11]. V_2 is defined as the point intercepting the ordinate axis with the charge slope. Then, the formula $Q_3 = I \times (V_2 - V_1/2)$ gives an over-estimation of the heat generation rate within the cell. Generally, the Equivalent Series Resistance (ESR) is a primary parameter of a capacitor defining the way this device works in circuits. The ESR is a convenient representation of the non-ideal behaviour of a capacitor with an equivalent electrical circuit using a lumped element model (see [5]). The resistance of the as defined circuit has a value equal to the resistance present in the capacitor. ESR is properly defined as the real resistive component of the complex impedance of the capacitor [3–5]. In practice, ESR can be evaluated by different ways such as reading of the potential offsets before charging and on charge (V_1 and V_2, respectively, see Fig. 9). Calorimetric ESR could be also defined as Q/I^2. Different equivalent resistances have been determined by the formulas (4)–(6) expressed as:

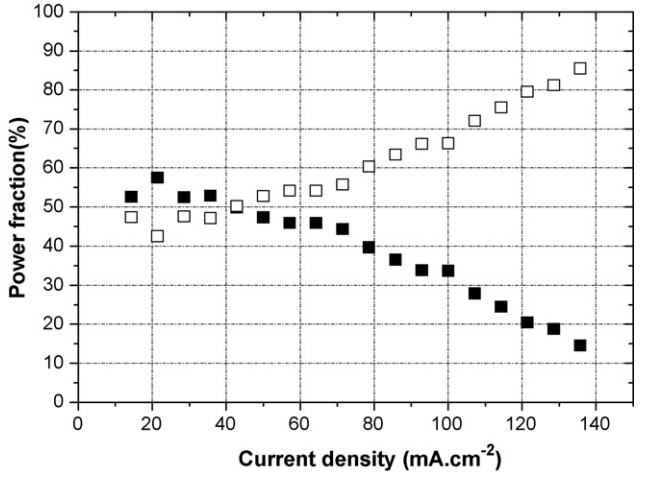

Fig. 11. Percentage of the heat generated within each component of the Double-Layer Capacitor cell as a function of the current density (□) within the separator Q_1/Q (■) within the carbon electrodes, Q_2/Q with $Q_2 = Q - Q_1$.

$$R = \frac{Q}{S \cdot j^2} \tag{4}$$

$$R_1 = \frac{Q_1}{S \cdot j^2} \tag{5}$$

$$R_3 = \frac{Q_3}{S \cdot j^2} \tag{6}$$

j is the current density and S the cell surface. The resistances (R, R_1, R_2) are given in $\Omega\,cm^2$. R refers to the calorimetric data. R_1 and R_3 refer to Q_1 and Q_3, respectively, related to the potential offsets. Fig. 12 presents the as defined resistance for the cell as a function of the current density. It was found that R varied between 4 and 8 $\Omega\,cm^2$ according to the current density. The error bars represented in Fig. 12 refers to the imprecision for measuring the potential offsets. At low current densities, the measurement of V_2 was inaccurate because the charge slope was changing with time. From Fig. 12, it can deduced that R_3 (charge resistance) overestimates and R_1 underestimates the heat generation rate over a wide current range.

4. Conclusion

A calorimetric technique was developed for measuring the average dissipated power by electrochemical cells under cycling by analyzing its transient temperature change.

Performance of the calorimetric technique was demonstrated on a symmetrical activated carbon cell with 1 M $N(C_2H_5)_4BF_4$ in propylene carbonate electrolyte having 0.25 F cm^{-2} as capacitance. Measurements have been performed at room temperature over a wide current range comprised between 0.01 and 0.15 A cm^{-2}. Following the current density, the power density was found between 2×10^{-3} and 70×10^{-3} W cm^{-2} for a loading pressure equal to 25 kg cm^{-2}. Equivalent resistance measured by the calorimetric technique was found to be between 4 and 8 Ω cm^2 according to the current density. Calorimetric measurements were found in good agreement with the energy balance of the cell deduced from the potential profiles and currents.

The as developed calorimetric technique offers a diagnostic route for electrochemical cells of energy storage devices such as capacitors and batteries. The technique can achieve a better understanding of the electrochemical processes and conversion efficiency of such devices, as well as study degradation and aging mechanisms taking place at electrodes.

Acknowledgements

French Agency for Research (ANR), Pôle de Compétivité Véhicule Haut de Gamme and French Agency for Energy (ADEME) are greatly acknowledged for supporting this work within the framework of the projects ABHYS and PowerTrain Booster.

References

[1] A. Burke, Ultracapacitors: why, how, and where is the technology, Journal of Power Sources 91 (2000) 37–50.
[2] A. Burke, R&D considerations for the performance and application of electrochemical capacitors, Electrochimica Acta 53 (2007) 1083–1091.
[3] B.E. Conway, Electrochemical Supercapacitors. Scientific Fundamentals and Technological Applications, Kluwer Academic Plenum Press, New York, 1999.
[4] J.R. Miller, A.F. Burke, Electrochemical capacitors: challenges and opportunities for real-world applications, The Electrochemical Society Interface 17 (2008) 53–57.
[5] J. Schiffer, D. Linzen, D.U. Sauer, Heat generation in double layer capacitors, Journal of Power Sources 160 (1) (2006) 765–772.
[6] J.R. Miller, Electrochemical capacitor thermal management issues at high cycling, Electrochemica Acta 52 (2006) 1703–1708.
[7] K. Onda, et al., Experimental study on heat generation behavior of small lithium-ion secondary batteries, Journal of the Electrochemical Society 150 (3) (2003) A285–A291.
[8] W. Lu, J. Prakash, In situ measurements of heat generation in a Li/mesocarbon microbead half-cell, Journal of the Electrochemical Society 150 (3) (2003) A262–A266.
[9] R. Knoedler, Calorimetric determination of the heat generation rate of sodium sulfur cells during discharge and charge, Electrochemical Science and Technology 131 (4) (1984) 946–950.
[10] B. Seguin, J.P. Gosse, J.P. Ferrieux, Calorimetric measurement and modeling of the equivalent series resistance of capacitors, The European Physical Journal, Applied Physics 8 (1999) 275–283.
[11] M.W. Verbrugge, P. Liu, Microstructural, analysis and mathematical modeling of electric double-layer supercapacitors, Journal of The Electrochemical Society 152 (2005) 79–87.
[12] P. Guillemet, Y. Scudeller, T. Brousse, Multilevel reduced order thermal modelling of electrochemical capacitors, Journal of Power Sources. 157 (2006) 630–640.
[13] M.J. Assael, S. Botsios, K. Gialou, I.N. Metaxa, Thermal conductivity of polymethyl methacrylate (PMMA) and Borosilicate Crown Glass BK7, International Journal of Thermophysics 26 (September (5)) (2005).